Available online at www.sciencedirect.com
ScienceDirect
Journal of Computational Physics 226 (2007) 1136–1151
JOURNAL OF COMPUTATIONAL PHYSICS
www.elsevier.com/locate/jcp

A numerical method for DNS/LES of turbulent reacting flows

Jeff Doom, Yucheng Hou, Krishnan Mahesh *

Department of Aerospace Engineering and Mechanics, University of Minnesota, United States

Received 2 May 2006; received in revised form 24 April 2007; accepted 15 May 2007
Available online 22 June 2007

Abstract

A spatially non-dissipative, implicit numerical method to simulate turbulent reacting flows over a range of Mach numbers, is described. The compressible Navier–Stokes equations are rescaled so that the zero Mach number equations are discretely recovered in the limit of zero Mach number. The dependent variables are co-located in space, and thermodynamic variables are staggered from velocity in time. The algorithm discretely conserves kinetic energy in the incompressible, inviscid, non-reacting limit. The chemical source terms are implicit in time to allow for stiff chemical mechanisms. The algorithm is readily extended to complex chemical mechanisms. Numerical examples using both simple and complex chemical mechanisms are presented.

Keywords: DNS; LES; Turbulent reacting flows; Non-dissipative; Implicit

1. Introduction

The direct numerical simulation (DNS) and large-eddy simulation (LES) of turbulent reacting flows are extremely challenging. Combustion involves a large number of chemical species, and associated chemical reactions. Different chemical reactions possess different time-scales, and different reaction zone thicknesses. Turbulence introduces its own range of length and time-scales. Furthermore the nonlinear nature of turbulence means that errors at the smaller scales have the potential to corrupt the large scales of the solution. Turbulent combustion can occur at very low Mach numbers (e.g. gas-turbine combustors at low pressures) or very high Mach numbers (e.g. scramjets). Very low Mach numbers imply numerical stiffness because of a large difference between the speed of sound and flow velocities, while very high Mach numbers result in shock waves, and their attendant problems. Desirable requirements for an algorithm to perform DNS/LES of turbulent reacting flows are therefore: (i) to handle high Reynolds numbers robustly and accurately, without the use of numerical dissipation, (ii) to handle acoustic stiffness efficiently, (iii) to deal with chemical stiffness, and combustion-induced large spatial gradients, and (iv) to deal with shock waves. This paper proposes an approach that deals with requirements (i)–(iii).

* Corresponding author. Tel.: +1 612 624 4175; fax: +1 612 626 1558.
E-mail address: mahesh@aem.umn.edu (K. Mahesh).

0021-9991/$ - see front matter © 2007 Published by Elsevier Inc.
doi:10.1016/j.jcp.2007.05.037

The proposed approach is an extension of the algorithm developed by Hou and Mahesh [1] for compressible flows without chemical reaction. The Hou and Mahesh algorithm is co-located in space, symmetric in both space and time, and hence non-dissipative. Motivated by the theoretical work of Thompson [2], and similar to the non-dimensionalization used by Bijl and Wesseling [3], and Van der Heul et al. [4], the Navier–Stokes equations are non-dimensionalized using an incompressible scaling for pressure, and the energy equation is interpreted as an equation for the divergence of velocity. A pressure-correction approach is used to constrain the divergence of the velocity field to satisfy the energy equation. The resulting system of equations analytically projects acoustic waves out, in the limit of zero Mach number. The discrete equations are fully implicit, and are constrained to discretely conserve kinetic energy in the limit of incompressible, inviscid flow. These features make the algorithm stable and accurate at high Reynolds numbers, and efficient and accurate at very low Mach numbers. Hou and Mahesh [1] show results for one-dimensional acoustic waves, a periodic shock tube, the incompressible Taylor problem, and inviscid isotropic turbulence on very coarse grids.

Most DNS/LES of turbulent reacting flows appear to either use the compressible Navier–Stokes equations with Pade spatial discretization, and explicit time-advancement (e.g. [5–9]), or the zero Mach number equations along with a pressure-projection approach (e.g. [10–13,15,16]). A second-order, staggered, implicit compressible algorithm was proposed by Wall et al. [14]. However, the Pade schemes become unstable at high Reynolds numbers; when explicit time-advancement is used, they require very small time-step at low Mach numbers, and for stiff chemical mechanisms. The zero Mach number equations are very efficient at low Mach numbers because they analytically project acoustic waves out; also along with implicit time-advancement they can resolve chemical stiffness efficiently. However, due to the complete absence of acoustic effects, they are not applicable to finite Mach number flows.

This paper therefore extends the Hou and Mahesh algorithm to include the effects of chemical reaction. The resulting algorithm treats the chemical source terms implicitly, solves the species equations in a segregated manner, which allows easy extension to multiple species and chemical reactions, and reduces to the zero Mach number equations in the limit of very small Mach number. The paper is organized as follows. Section 2 describes the non-dimensional governing equations, and their behavior in the limit of very small Mach number. The discrete scheme is described in Section 3. The positioning of variables, and details of the pressure-correction approach are discussed. Section 4 presents some numerical examples. Results are shown for a laminar premixed flame, laminar unstrained diffusion flame, reacting two-dimensional jets, and a turbulent non-premixed flame. Both simple and complex chemical mechanisms are considered. A brief summary in Section 5 concludes the paper.

2. Governing equations

The governing equations are the compressible, reacting Navier–Stokes equation for an ideal gas:

$$\frac{\partial \rho^d}{\partial t^d} + \frac{\partial \rho u_j^d}{\partial x_j^d} = 0, \tag{1}$$

$$\frac{\partial \rho^d Y_k^d}{\partial t^d} + \frac{\partial \rho Y_k^d u_j^d}{\partial x_j^d} = \frac{\partial}{\partial x_j^d}\left(\rho^d D_k^d \frac{\partial Y_k^d}{\partial x_j^d}\right) + \dot{\omega}_k^d, \tag{2}$$

$$\frac{\partial \rho^d u_i^d}{\partial t^d} + \frac{\partial \rho^d u_i^d u_j^d}{\partial x_j^d} = -\frac{\partial p^d}{\partial x_i^d} + \frac{\partial \tau_{ij}^d}{\partial x_j^d}, \tag{3}$$

$$\frac{\partial \rho^d E^d}{\partial t^d} + \frac{\partial \left(\rho^d E^d + p^d\right) u_j^d}{\partial x_j^d} = \frac{\partial \tau_{ij}^d u_i^d}{\partial x_j^d} + \frac{\partial}{\partial x_j^d}\left(\mu^d \frac{c_p^d}{Pr} \frac{\partial T^d}{\partial x_j^d}\right) + \sum_{k=1}^{N} Q_k^d \dot{\omega}_k^d \tag{4}$$

$$p^d = \rho^d R^d T^d = \rho^d \frac{R_u}{W^d} T^d. \tag{5}$$

where the superscript 'd' denotes the dimensional value. The variables ρ, p, Y_k and u_i denote the density, pressure, mass fraction of species k and velocities, respectively. $E = c_v T^d + u_i^d u_i^d/2$ denotes the total energy per unit

mass and $\tau_{ij} = \mu^d \left(\frac{\partial u_i^d}{\partial x_j^d} + \frac{\partial u_j^d}{\partial x_i^d} - \frac{2}{3} \frac{\partial u_k^d}{\partial x_k^d} \delta_{ij} \right)$ is the viscous stress tensor. D_k^d, c_p and Pr denote the diffusion coefficient of the kth species, specific heat at constant pressure and the Prandtl number. For the source term, Q_k^d is the heat of reaction per unit mass and $Q_k^d \dot{\omega}_k^d$ is the heat release due to combustion for the 'kth' species. $\dot{\omega}_k$ is the mass reaction rate for the kth species. R_u is the universal gas constant and W^d is the mean molecular weight of the mixture defined as: $\frac{1}{W^d} = \Sigma_{k=1}^{N} \frac{Y_k}{W_k}$. The source term is modeled using the Arrhenius law in this paper.

The reacting governing equation are non-dimensionalized as follows. Let ρ_r, Y_r, L, and T_r denote the reference density, mass fraction, length and temperature, respectively. The reference velocity, dynamic viscosity and pressure are denoted by u_r, μ_r and p_r, respectively. The ratio $\gamma = \frac{c_p^d}{c_v^d}$ is assumed to be constant (e.g. [6]). This yields the following non-dimensional variables:

$$\rho = \frac{\rho^d}{\rho_r}, \quad u_i = \frac{u_i^d}{u_r}, \quad t = \frac{t^d}{L/u_r}, \quad \mu = \frac{\mu^d}{\mu_r}, \quad p = \frac{p^d - p_r}{\rho_r u_r^2}, \tag{6}$$

$$T = \frac{T^d}{T_r}, \quad M_r = \frac{u_r}{a_r} = \frac{u_r}{\sqrt{\gamma R_r T_r}}, \quad p_r = \rho_r R_r T_r, \tag{7}$$

$$Y_k = \frac{Y_k^d}{Y_r}, \quad D_k = \frac{D_k^d}{u_r L}, \quad \dot{\omega}_k = \frac{L \dot{\omega}_k^d}{u_r \rho_r Y_r}, \quad Q_k = \frac{Y_r Q_k^d}{c_{p,r} T_r}, \tag{8}$$

$$R_r = \frac{R_u}{W_r}, \quad \text{and} \quad W = \frac{W^d}{W_r}. \tag{9}$$

Note that pressure is non-dimensionalized using an incompressible scaling. This non-dimensionalization is motivated by Thompson [2], Bijl and Wesseling [3], Van der Heul et al. [4] and Hou and Mahesh [1]. Therefore, the non-dimensional governing equations for reacting flows are:

$$\frac{\partial \rho}{\partial t} + \frac{\partial \rho u_j}{\partial x_j} = 0, \tag{10}$$

$$\frac{\partial \rho Y_k}{\partial t} + \frac{\partial \rho Y_k u_j}{\partial x_j} = \frac{1}{ReSc_k} \frac{\partial}{\partial x_j} \left(\mu \frac{\partial Y_k}{\partial x_j} \right) + \dot{\omega}_k, \tag{11}$$

$$\frac{\partial \rho u_i}{\partial t} + \frac{\partial \rho u_i u_j}{\partial x_j} = -\frac{\partial p}{\partial x_i} + \frac{1}{Re} \frac{\partial \tau_{ij}}{\partial x_j}, \tag{12}$$

$$M_r^2 \left[\frac{\partial}{\partial t} \left(p + \frac{\gamma - 1}{2} \rho u_i u_i \right) + \frac{\partial}{\partial x_j} \left(\gamma p + \frac{\gamma - 1}{2} \rho u_i u_i \right) u_j \right] + \frac{\partial u_j}{\partial x_j} = \frac{(\gamma - 1) M_r^2}{Re} \frac{\partial \tau_{ij} u_j}{\partial x_j} + \frac{1}{RePr} \frac{\partial}{\partial x_j} \left(\frac{\mu}{W} \frac{\partial T}{\partial x_j} \right) + \sum_{k=1}^{N} Q_k \dot{\omega}_k \tag{13}$$

$$\frac{\rho T}{W} = \gamma M_r^2 p + 1. \tag{14}$$

where Sc_k is the Schmidt number for the kth species. When the reference Mach number is zero, the non-dimensional reacting governing equations reduce to

$$\frac{\partial \rho}{\partial t} + \frac{\partial \rho u_j}{\partial x_j} = 0, \tag{15}$$

$$\frac{\partial \rho u_i}{\partial t} + \frac{\partial \rho u_i u_j}{\partial x_j} = -\frac{\partial p}{\partial x_i} + \frac{1}{Re} \frac{\partial \tau_{ij}}{\partial x_j}, \tag{16}$$

$$\frac{\partial \rho Y_k}{\partial t} + \frac{\partial \rho Y_k u_j}{\partial x_j} = \frac{1}{ReSc_k} \frac{\partial}{\partial x_i} \left(\mu \frac{\partial Y_k}{\partial x_j} \right) + \dot{\omega}_k, \tag{17}$$

$$\frac{\partial u_j}{\partial x_j} = \frac{1}{RePr} \frac{\partial}{\partial x_j} \left(\frac{\mu}{W} \frac{\partial T}{\partial x_j} \right) + \sum_{k=1}^{N} Q_k \dot{\omega}_k, \tag{18}$$

$$\frac{\rho T}{W} = 1. \tag{19}$$

Notice that the divergence of velocity equals the sum of the terms involving thermal conduction and heat release. If the density is constant and there is no heat release, the energy equation reduces to the incompressible continuity equation. In the presence of heat release, the zero Mach number reacting equations [10] are obtained. Most projection methods for the zero Mach number equations project the momentum ρu_i to satisfy the momentum equation. Here, the velocity is projected to satisfy the energy equation. The reaction source term can be quite complicated for multiple species, and is discussed in more detail in Section 3.1.

3. Discretization

Density, pressure, and temperature are staggered in time from velocity by Hou and Mahesh [1]. The mass fraction of species k are similarly staggered in time here. The thermodynamic variables and mass fraction of species k are advanced in time from $t+\frac{1}{2}$ to $t+\frac{3}{2}$, illustrated in Fig. 1. The variables are co-located in space, to allow easy application to unstructured grids.

Integrating over the control volume and applying Gauss's theorem yields the discrete governing equations. The discrete continuity and species equations are

$$\frac{\rho_{cv}^{t+\frac{3}{2}}-\rho_{cv}^{t+\frac{1}{2}}}{\Delta t}+\frac{1}{V}\sum_{\text{faces}}\rho_{\text{faces}}^{t+1}V_N^{t+1}A_{\text{face}}=0 \tag{20}$$

and

$$\frac{(S_k)_{cv}^{t+\frac{3}{2}}-(S_k)_{cv}^{t+\frac{1}{2}}}{\Delta t}+\frac{1}{V}\sum_{\text{faces}}(S_k)_{\text{faces}}^{t+1}V_N^{t+1}A_{\text{face}}=\frac{1}{ReSc_k}\frac{1}{V}\sum_{\text{faces}}\left(\mu\left[\frac{1}{\rho}\frac{\partial S_k}{\partial x_j}-\frac{S_k}{\rho^2}\frac{\partial \rho}{\partial x_j}\right]\right)_{\text{faces}}^{t+1}N_jA_{\text{face}}+\dot{\omega}_k^{t+1}. \tag{21}$$

where ρ_{cv} denotes $\rho_{i,j,k}$ and Σ_{faces} denotes summation over all the faces of the control volume. ρ_{faces} and v_N denotes the density and normal face velocity at each face. Note that $S_k=\rho Y_k$. The variables $(S_k)_{\text{faces}}$ denotes the species at the face and N_j is the outward normal vector at the face. The variables V and A_{face} denote the volume of the control volume and the area of the face. The discrete momentum equation is:

$$\frac{(g_i)_{cv}^{t+1}-(g_i)_{cv}^{t}}{\Delta t}+\frac{1}{V}\sum_{\text{faces}}(g_i)_{\text{faces}}^{t+\frac{1}{2}}V_N^{t+\frac{1}{2}}A_{\text{face}}=-\frac{1}{V}\sum_{\text{faces}}p_{\text{faces}}^{t}N_jA_{\text{face}}+\frac{1}{Re}\frac{1}{V}\sum_{\text{faces}}(\tau_{ij})_{\text{face}}^{t+\frac{1}{2}}N_jA_{\text{face}}. \tag{22}$$

Here, $g_i=\rho u_i$ denotes the momentum in the i direction and τ_{ij} is the stress tensor. The discrete energy equation is given by:

$$\begin{aligned}&M_r^2\left[\frac{\partial}{\partial t}\left(p_{cv}+\frac{\gamma-1}{2}\rho u_iu_i\right)^{t+\frac{1}{2}}+\frac{1}{V}\sum_{\text{faces}}\left(\gamma p_{cv}+\frac{\gamma-1}{2}\rho u_iu_i\right)_{\text{face}}^{t+\frac{1}{2}}\cdot v_N^{t+\frac{1}{2}}A_{\text{face}}\right]+\frac{1}{V}\sum_{\text{face}}v_N^{t+\frac{1}{2}}A_{\text{face}}\\&=\frac{(\gamma-1)M_r^2}{Re}\frac{1}{V}\sum_{\text{faces}}(\tau_{ij}u_i)_{\text{face}}^{t+\frac{1}{2}}N_jA_{\text{face}}+\frac{1}{RePr}\frac{1}{V}\sum_{\text{faces}}\left(\frac{\mu}{W}\frac{\partial T^{t+\frac{1}{2}}}{\partial N}\right)A_{\text{face}}+\sum_{k=1}^{N}Q_k\dot{\omega}_k^{t+\frac{1}{2}}.\end{aligned} \tag{23}$$

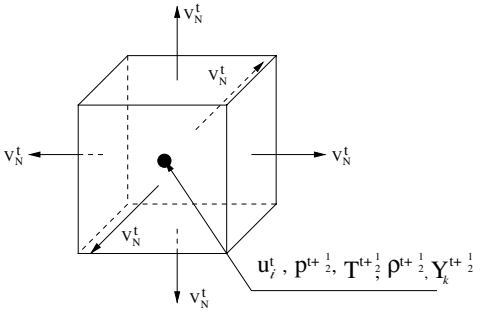

Fig. 1. Storage of variables.

The algorithm solves each equation separately. This allows one to add multiple species with relative ease, which allows easy extension to complex chemistry. Note that the chemical source term is handled implicitly. Details of the implicit procedure are described in Section 3.1. The algorithm is a pressure-correction method. An important feature is that the face-normal velocities are projected to satisfy the constraint on the divergence which is determined by the energy equation. At small Mach number, this feature ensures that the velocity field is discretely divergence free. This is in contrast to most approaches that project the momentum which is constrained by the continuity equation. A predictor–corrector approach is used to solve the momentum and energy equation:

$$p^{t+\frac{3}{2},k+1} = p^{t+\frac{3}{2},k} + \delta p. \tag{24}$$

The corrector step is the difference between the predictor equation and the exact equation which is defined as

$$g_{i,cv}^{t+1,k+1} = g_{i,cv}^{*} - \frac{\Delta t}{4}\left(\frac{\partial \delta p}{\partial x_i}\right)_{cv}, \tag{25}$$

$$u_{i,cv}^{t+1,k+1} = u_{i,cv}^{*} - \frac{\Delta t}{4\rho_{cv}^{t+1}}\left(\frac{\partial \delta p}{\partial x_i}\right)_{cv}. \tag{26}$$

Substituting Eq. (26) into the nonlinear term $u_i u_i$ converts kinetic energy into an equation for δp which is:

$$(u_i u_i)^{t+1,k+1} = \left(u_i^{*} - \frac{\Delta t}{4\rho_{cv}^{t+1}}\left(\frac{\partial \delta p}{\partial x_i}\right)\right)\left(u_i^{*} - \frac{\Delta t}{4\rho_{cv}^{t+1}}\left(\frac{\partial \delta p}{\partial x_i}\right)\right) = u_i^{*}u_i^{*} - \frac{\Delta t}{2\rho^{t+1}}u_i^{*}\frac{\partial \delta p}{\partial x_i} + \mathrm{O}(\delta p^2). \tag{27}$$

Eq. (27) is then substituted into Eq. (23), and yields a discrete energy equation in terms of δp. Note that δp is the difference between iterations, which implies that δp converges to zero at each time-step. This allows the high order terms in Eq. (27) to be neglected. The implementation to solve the following discrete equations are to initialize the outer loop:

$$\rho^{t+\frac{3}{2},0} = \rho^{t+\frac{1}{2}}, \quad u_i^{t+1,0} = u_i^{t}, \quad T^{t+\frac{3}{2},0} = T^{t+\frac{1}{2}}, \quad v_N^{t+1,0} = v_N^{t}, \quad S_k^{t+\frac{3}{2},0} = S_k^{t+\frac{1}{2}}. \tag{28}$$

The next procedure is to advance the continuity Eq. (20), then advance the species Eq. (21). Once the species is advance, advance the momentum Eq. (22), then obtain v_N^{*} by interpolation. After obtaining v_N^{*}, the next step is to solve the pressure-correction equation (23). Use the corrector steps to update pressure (24), momentum (25) and the velocities (26), then check the convergence for the pressure, momentum, density, and species between outer loop iterations.

3.1. Implicit source term

Consider a chemical system of N species reacting through M reactions denoted as [6]:

$$\sum_{j=1}^{N} \nu'_{kj}\mu_k \rightleftharpoons \sum_{j=1}^{M} \nu''_{kj}\mu_k \tag{29}$$

for $j = 1,M$ where μ_k is a symbol for species k. ν'_{kj} and ν''_{kj} are the stoichiometric coefficients of species k for j reactions. The reaction term is defined as:

$$\dot{\omega}_k = W_k \sum_{j=1}^{M} \nu_{kj}\widehat{Q}_j \tag{30}$$

where

$$\widehat{Q}_j = \underbrace{K_{ij}\prod_{k=1}^{N}\left(\frac{\rho Y_k}{W_k}\right)^{\nu'_{kj}}}_{\text{forward reaction}} - \underbrace{K_{rj}\prod_{k=1}^{N}\left(\frac{\rho Y_k}{W_k}\right)^{\nu''_{kj}}}_{\text{reverse reaction}}. \tag{31}$$

Using the empirical Arrhenius law,

$$K_{ij} = A_{ij}T^{\beta_j}\exp\left(-\frac{E_j}{RT}\right) = A_{ij}T^{\beta_j}\exp\left(-\frac{T_{a_j}}{T}\right). \tag{32}$$

Therefore, the source term is:

$$\dot{\omega}_k = W_k\sum_{j=1}^{M}\nu_{kj}\left[A_{ij}T^{\beta_j}\exp\left(-\frac{T_{a_j}}{T}\right)\prod_{k=1}^{N}\left(\frac{S_k}{W_k}\right)^{\nu'_{kj}}\right] - W_k\sum_{j=1}^{M}\nu_{kj}\left[A_{rj}T^{\beta_j}\exp\left(-\frac{T_{a_j}}{T}\right)\prod_{k=1}^{N}\left(\frac{S_k}{W_k}\right)^{\nu''_{kj}}\right]. \tag{33}$$

The discrete form of Eq. (33) is:

$$\begin{aligned}\dot{\omega}_k^{t+1} = {} & W_k\sum_{j=1}^{M}\nu_{kj}\left[A_{ij}T_{cv}^{\beta_j,t+1}\exp\left(-\frac{T_{a_j}}{T_{cv}^{t+1}}\right)\prod_{k=1}^{N}\left(\frac{S_{k,cv}^{t+\frac{3}{2}}+S_{k,cv}^{t+\frac{1}{2}}}{2W_k}\right)^{\nu'_{kj}}\right]\\ & - W_k\sum_{j=1}^{M}\nu_{kj}\left[A_{rj}T_{cv}^{\beta_j,t+1}\exp\left(-\frac{T_{aj}}{T_{cv}^{t+1}}\right)\prod_{k=1}^{N}\left(\frac{S_{k,cv}^{t+\frac{3}{2}}+S_{k,cv}^{t+\frac{1}{2}}}{2W_k}\right)^{\nu''_{kj}}\right].\end{aligned} \tag{34}$$

Substituting Eq. (34) into Eq. (21) for $\dot{\omega}_k^{t+1}$ yields:

$$\begin{aligned}&\frac{(S_k)_{cv}^{t+\frac{3}{2}}-(S_k)_{cv}^{t+\frac{1}{2}}}{\Delta t}+\frac{1}{V}\sum_{\text{faces}}(S_k)_{\text{faces}}^{t+1}V_N^{t+1}A_{\text{face}}\\ &\quad=\frac{1}{ReSc_k}\frac{1}{V}\sum_{\text{faces}}\left(\mu\left[\frac{1}{\rho}\frac{\partial S_k}{\partial x_j}-\frac{S_k}{\rho^2}\frac{\partial\rho}{\partial x_j}\right]\right)_{\text{faces}}^{t+1}N_jA_{\text{face}}\\ &\qquad+W_k\sum_{j=1}^{M}\nu_{kj}\left[A_{ij}T_{cv}^{\beta_j,t+1}\exp\left(-\frac{T_{a_j}}{T_{cv}^{t+1}}\right)\prod_{k=1}^{N}\left(\frac{S_{k,cv}^{t+\frac{3}{2}}+S_{k,cv}^{t+\frac{1}{2}}}{2W_k}\right)^{\nu'_{kj}}\right]\\ &\qquad-W_k\sum_{j=1}^{M}\nu_{kj}\left[A_{rj}T_{cv}^{\beta_j,t+1}\exp\left(-\frac{T_{a_j}}{T_{cv}^{t+1}}\right)\prod_{k=1}^{N}\left(\frac{S_{k,cv}^{t+\frac{3}{2}}+S_{k,cv}^{t+\frac{1}{2}}}{2W_k}\right)^{\nu''_{kj}}\right].\end{aligned} \tag{35}$$

Eq. (35) can be represented as

$$a_pS_{cv}^{t+\frac{3}{2}}+\sum_{nb}a_{nb}S_{nb}^{t+\frac{3}{2}}=\text{RHS}. \tag{36}$$

where *nb* are the neighbors of the *cv*. A parallel, algebraic multi-grid approach is used to solve the system of algebraic equations. The structured grid interface of the *Hypre* library (Lawrence Livermore National Laboratory 2003) is used. Three different examples of the implicit source term are described below. If $N=1$, $M=1$ and only forward reaction is assumed, this implies that

$$\widehat{Q}_1 = A_{11}T^{\beta_1}\exp\left(-\frac{T_{a_1}}{T}\right)\left(\frac{\rho Y_1}{W_1}\right)^{\nu'_{11}} \tag{37}$$

which implies

$$\dot{\omega}_1 = W_1A_{11}\nu_{11}T^{\beta_1}\exp\left(-\frac{T_{a_1}}{T}\right)\left(\frac{\rho Y_1}{W_1}\right)^{\nu'_{11}}. \tag{38}$$

Note that for a one-step premixed flame:

$$\dot{\omega} = B_\rho Y\exp\left(\frac{-T_a}{T^d}\right) \tag{39}$$

which upon discretization yields:

$$\dot{\omega}^{t+1} = B\frac{S_{cv}^{t+\frac{3}{2}} + S_{cv}^{t+\frac{1}{2}}}{2}\exp\left(\frac{-T_a}{T_{cv}^{t+1}}\right). \tag{40}$$

Eq. (40) is the source term used in Section 4.1. Consider a two-step reaction from Chen et al. [20] and Mahalingam et al. [18] given by:

$$\begin{aligned} A + B &\rightarrow I \\ A + I &\rightarrow P. \end{aligned} \tag{41}$$

Note that A is the fuel, B is the oxidizer, I is the intermediate step, and P is the product. The source term for species A is defined as:

$$\dot{\omega}_k = B_1\rho Y_A \rho Y_B \exp\left(-\frac{T_{a_1}}{T}\right) + B_2\rho Y_A \rho Y_I \exp\left(-\frac{T_{a_2}}{T}\right). \tag{42}$$

The discrete form is:

$$\dot{\omega}_k = B_1\frac{S_{A,cv}^{t+\frac{3}{2}} + S_{A,cv}^{t+\frac{1}{2}}}{2}S_{B,cv}^{t+1}\exp\left(-\frac{T_{a_1}}{T_{cv}^{t+1}}\right) + B_2\frac{S_{A,cv}^{t+\frac{3}{2}} + S_{A,cv}^{t+\frac{1}{2}}}{2}S_{I,cv}^{t+1}\exp\left(-\frac{T_{a_2}}{T_{cv}^{t+1}}\right). \tag{43}$$

This implicit source term is used in Section 4.4. Note that the other species are handled in a similar manner. The final example is a nonlinear source term which is used in 4.2 and 4.3:

$$\dot{\omega}_k = -A\rho^{\nu_F+\nu_O}Y_F^{\nu_F}Y_O^{\nu_O}\exp\left(-\frac{T_a}{T}\right). \tag{44}$$

Let $\nu_F = 2$ and $\nu_O = 1$. This implies:

$$\dot{\omega}_k = -A\rho^{2+1}Y_F^2 Y_O^1 \exp\left(-\frac{T_a}{T}\right) = -AS_F^2 S_O^1 \exp\left(-\frac{T_a}{T}\right) \tag{45}$$

where F is the fuel and O is the oxidizer. The discrete equation for the fuel species is:

$$\dot{\omega}_k^{t+1} = -A\underbrace{\left[\frac{S_{F,cv}^{t+\frac{3}{2}} + S_{F,cv}^{t+\frac{1}{2}}}{2}\right]}_{(1)}\underbrace{S_{F,cv}^{t+1}}_{(2)}S_{O,cv}^{t+1}\exp\left(-\frac{T_a}{T_{cv}^{t+1}}\right). \tag{46}$$

The nonlinear source term is linearized by only solving for term (1) and term (2) is from previous iterations. The outer loop ensures that the nonlinear corrections converge to zero.

3.2. Zero Mach number limit

The governing equations analytically reduce to the zero Mach number equations, as shown in Section 2. Since the dependent variables are spatially co-located, it appears that the pressure-projection step might result in odd–even decoupling. It is well known that the incompressible equations require staggering, temporal dissipation, or low order basis functions for pressure, to avoid odd–even decoupling. However, note that the inner loop in the proposed algorithm uses nearest neighbors for the pressure equation; it therefore does not suffer from odd–even decoupling. The tolerance assigned to the outer loop can in practice, be controlled to obtain low Mach number solutions. However, a more reliable approach which explicitly introduces temporal biasing is that proposed by [14], which is now used here.

Recall that the pressure gradient term in the momentum equation is defined as

$$\frac{\partial p^{t+\frac{1}{2}}}{\partial x_i} = \frac{1}{4}\frac{\partial p^{t-\frac{1}{2}}}{\partial x_i} + \frac{1}{2}\frac{\partial p^{t+\frac{1}{2}}}{\partial x_i} + \frac{1}{4}\frac{\partial p^{t+\frac{3}{2}}}{\partial x_i}. \tag{47}$$

Temporal biasing can be introduced by computing the pressure gradient as

$$\frac{\partial p^{t+\frac{1}{2}}}{\partial x_i} = \left(\frac{1}{4}-\epsilon\right)\frac{\partial p^{t-\frac{1}{2}}}{\partial x_i} + \frac{1}{2}\frac{\partial p^{t+\frac{1}{2}}}{\partial x_i} + \left(\frac{1}{4}+\epsilon\right)\frac{\partial p^{t+\frac{3}{2}}}{\partial x_i}. \tag{48}$$

Taylor expansion of the pressure at time level $t+\frac{1}{2}$ yields:

$$\left(\frac{1}{4}-\epsilon\right)\frac{\partial p^{t-\frac{1}{2}}}{\partial x_i} + \frac{1}{2}\frac{\partial p^{t+\frac{1}{2}}}{\partial x_i} + \left(\frac{1}{4}+\epsilon\right)\frac{\partial p^{t+\frac{3}{2}}}{\partial x_i} = \frac{\partial}{\partial x_i}\left(p^{t+\frac{1}{2}} + 2\epsilon\Delta t\frac{\partial p^{t+\frac{1}{2}}}{\partial t}\right) + \mathrm{O}(\Delta t^2). \tag{49}$$

i.e., the leading order term is first-order in time, for a given ϵ in Eq. (49). Alternate biased formulations of the pressure gradient can be used, but as the Taylor series expansion shows, using ϵ of the order of Δt would be the most time-accurate.

Two examples are used to illustrate the low Mach number behavior of the algorithm. The first example is the non-reacting Taylor problem discussed in more detail in Hou and Mahesh [1], while the second example corresponds to a synthetic premixed flame for which an analytical solution is obtained: i.e.

$$T = \sin x + 2, \quad Y = \sin x + 2, \quad u = \sin x + 2, \quad p = \frac{4}{3}\cos x - \sin x, \quad \rho = 1/T, \quad \dot{\omega} = -\cos x - \sin x. \tag{50}$$

For the Taylor problem, Δt was set to 0.001 and for the reacting case Δt was 0.0001. Fig. 2a show the variation of acoustic CFL, and number of outer loop iterations with M_r, respectively. M_r varies from 10^{-2} to 10^{-5} for the Taylor problem, and from 10^{-3} to 10^{-6} for the reacting case. Solutions were also obtained for M_r equal to zero, but are not shown due to the use of logarithmic axes. Here, ϵ was chosen to be 0.05. Note that the acoustic CFL varies inversely with M_r; i.e. low Mach numbers can be computed at fixed time-step. Also, note that the number of outer loop iterations at low Mach number is only twice that at finite Mach number, and remains constant at very low Mach numbers.

4. Results

The algorithm is applied to a one-dimensional steady laminar premixed flame in Section 4.1 and an unsteady laminar diffusion flame in Section 4.2. These two examples illustrate the ability to handle large heat release at low Mach number. Section 4.3 considers a steady two-dimensional laminar reacting jet flame with large heat release at low Mach number. Section 4.4 considers three-dimensional numerical simulations of

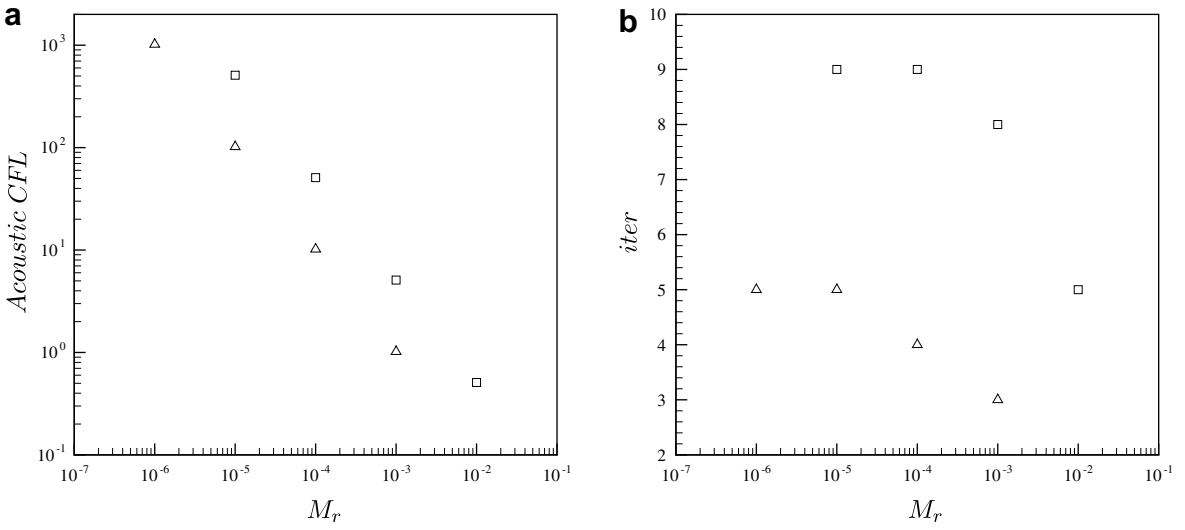

Fig. 2. Variation of (a) acoustic CFL and (b) number of outer loop iterations with M_r. Taylor □, Reacting △.

turbulent non-premixed flames with finite rate chemistry. This problem illustrates application to turbulence and finite Mach number. The examples involving simple chemistry, assume that the mean molecular weight is constant. The final example in Section 4.5 illustrates application to complex chemistry for H_2–O_2 combustion using a 9 species, 19 reaction mechanism from Mueller et al. [21].

4.1. Laminar premixed flame

An irreversible, one-step, laminar premixed flame is considered as an example of a low Mach number reacting flow. The reaction is given by $R \rightarrow P$ where R is the reactant and P is the product. The reaction source term is that proposed by Echekki and Ferziger [17]. It approximates the Arrhenius source term, and is useful for validation, in that it permits analytical solution. The reaction model is defined as:

$$\dot{\omega} = \begin{cases} 0 & \text{for } \Theta < \Theta_c, \\ \beta(\beta-1)(\Theta-1) & \text{otherwise.} \end{cases} \tag{51}$$

The corresponding analytical solution is given by:

$$\Theta = \begin{cases} \left(1-\beta^{-1}\right)\exp(x) & \text{for } x \leqslant 0, \\ 1-\beta^{-1}\exp[(1-\beta)x] & \text{for } x \geqslant 0. \end{cases} \tag{52}$$

Generally, β is the order of 10 for hydrocarbon combustion [17].

Fig. 3a shows computed results for a premixed flame where $\beta = 10$, $\alpha = 0.8$, and the inflow Mach number is equal to 0.01. The Echekki and Ferziger source term is used. The inflow velocity is set equal to the flame speed, and the solution is initialized using a hyperbolic tangent profile for the temperature distribution. The inlet boundary condition for temperature, density, species and velocity are set to one. Zero derivative boundary conditions are specified at the outflow. Boundary conditions based on characteristic analysis are not specified, due the simplicity of the solution at the boundaries, and the use of 'sponge' boundary conditions at both inflow and outflow boundaries to absorb acoustic waves that are generated by the initial transient. A cooling term, $-\sigma(U - U_{\text{ref}})$ is added to the right hand side of the governing equations over the sponge zone, whose length is 10% of the domain. Here U and U_{ref} denote the vector of conservative variables and the 'reference' solution, respectively. The coefficient σ is a polynomial function defined as:

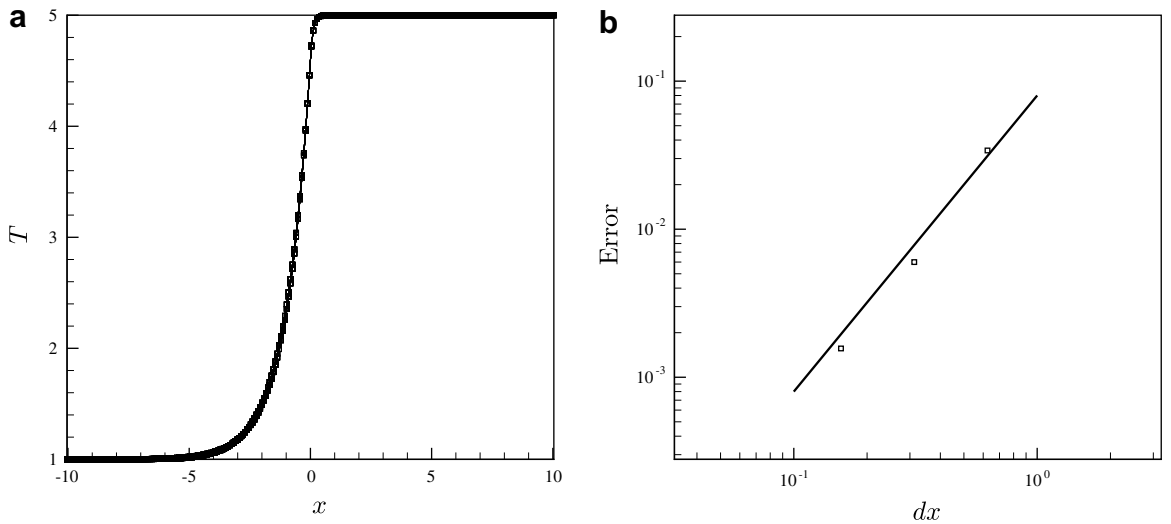

Fig. 3. (a) Comparison of computed temperature to analytical solution for a laminar premixed flame. □ analytic solution, —— numerical solution. $Sc = Re = Pr = 1$, $\beta = 10$, $\alpha = 0.8$, $M_r = 0.01$, (b) spatial order of accuracy. □ Algorithm, —— second-order, $Sc = Re = Pr = 1$, $\alpha = 0.5$, $\beta = 2$, $M_r = 0.01$.

$$\sigma(x) = A_s \frac{(x - x_s)^n}{(L_x - x_s)^n}, \tag{53}$$

where x_s and L_x denotes the start of the sponge and the length of the domain. n and A_s are equal to three. After a brief transient, the solution settles into a steady state which is shown in Fig. 3a. The computed and analytical solutions seem to agree well.

Fig. 3b shows results from a grid-convergence study. The time-step is fixed at $\mathrm{d}t = 0.001$, and the grid size is equal to 32, 64, and 128. Note that second-order accuracy is obtained. The computation cost is as follows. For $Nx = 128$, 10 outer loop iterations, one continuity equation iteration, five iterations for each momentum equation, one iteration for species and three iterations for the pressure-correction equation are required. The corresponding residual for the outer loop is 10^{-8} and 10^{-15} for the inner loop.

4.2. Laminar diffusion flame

A one-dimensional, unstrained diffusion flame with one-step chemistry is computed. This problem applies the algorithm to a high Damkohler number (defined as the ratio of flow time scale to chemical time scale, $Da = 50 \times 10^6$) chemical mechanism and very low Mach number. The chemistry model is a one-step reaction defined as

$$\nu_F Y_F + \nu_O Y_O \rightarrow \nu_P Y_P, \tag{54}$$

where Y_F, Y_O and Y_P are the mass fractions of the fuel, oxidizer and products. The computed solution is compared to an asymptotic solution developed by Cuenot and Poinsot [5]. Their analysis is applicable to diffusion flames with variable density, non-uniform Lewis number, and finite rate chemistry. Cuenot and Poinsot studied unsteady unstrained, steady strained and unsteady strained H_2–O_2 flames. Case 2 from their paper corresponds to an unsteady, unstrained flame, and was chosen for comparison. Table 1 lists the conditions for case 2.

Note that Le_F and Le_O denote the Lewis number for fuel and oxidizer. $T_{F,0}$ and $T_{O,0}$ are the initial temperatures of the fuel and oxidizer. Φ is the equivalence ratio which is defined as

$$\Phi = s \frac{Y_{F,0}}{Y_{O,0}} = \frac{\nu_O W_O}{\nu_F W_F} \frac{Y_{F,0}}{Y_{O,0}}, \tag{55}$$

where s is the stoichiometric ratio. The equivalence ratio is used to determine if the mixture is rich ($\Phi > 1$), lean ($\Phi < 1$) or stoichiometric ($\Phi = 1$). ν_F and ν_O denote the stoichiometric coefficients of the species. A is the pre-exponential factor and T_a is the activation temperature. The Arrhenius reaction rate is defined by Cuenot and Poinsot as

$$\dot{\omega}_k = -\nu_k W_k A \left(\frac{\rho Y_F}{W_F}\right)^{\nu_F} \left(\frac{\rho Y_O}{W_O}\right)^{\nu_O} \exp\left(-\frac{T_a}{T}\right). \tag{56}$$

Fig. 4 is a comparison of the computed solution to the asymptotic solution from Cuenot and Poinsot. The asymptotic solution was used to initialize the temperature, fuel mass fraction, and oxidizer mass fraction. The initial velocity profile was calculated from the energy equation. The initial pressure remains uniform in the flame and the initial density is obtained from temperature. Initially the reaction rate is zero because the asymptotic solution assumes infinitely fast chemistry. However, the simulation involves (fast) finite rate chemistry. Therefore, the reaction rate rapidly recovers in the simulation (Cuenot and Poinsot). The inlet boundary condition for temperature, density, and mass fraction of fuel are set to one. Mass fraction of oxidizer and velocity are set to zero. Zero derivative boundary conditions are specified at the

Table 1
Test condition

Case	Le_F	$T_{F,0}$ (K)	Le_O	$T_{O,0}$ (K)	Φ	ν_F	ν_O	A	T_a (K)	Q/c_p (K)	Re
2	1	300	1	300	8	2	1	10^8	3600	6000	10,000

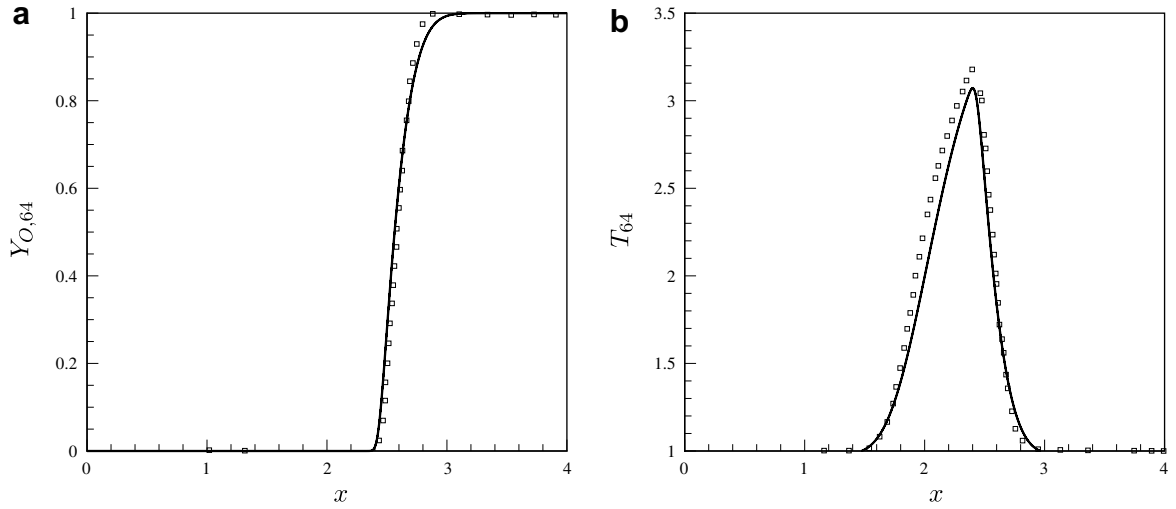

Fig. 4. Comparison of asymptotic solution to numerical solution for a laminar diffusion flame. (a) Mass fraction of oxidizer and (b) temperature profile at a non-dimensional time of 64. □ asymptotic solution, —— numerical solution, $M_r = 0.001$, $Sc_k = 1$, $Pr = 1$.

outflow. The initial time was set at $ct/L = 20$ and the solution was advanced to a time of $ct/L = 64$. Again, the 'sponge' boundary conditions were used at both inflow and outflow boundaries to absorb acoustic waves generated by the initial transient. The sponge zone is 10% of the domain. Also, the flow Mach number is 0.001 and the grid used 512 points. Reasonable agreement between computed and asymptotic solution is obtained.

4.3. Laminar 2D jet flame

A steady two-dimensional reacting laminar jet flame from Poinsot and Veynante [6] is considered. This problem illustrates the ability to handle large heat release and nearly incompressible flow for a one-step diffusion flame with a Damkohler number of 50×10^6. From Poinsot and Veynante [6], if one assumes constant mass flow rate ($\rho u = \text{constant}$), $v = w = 0$ and $\rho D = \text{constant}$, then the mixture fraction ζ satisfies:

$$\rho_F u_f \frac{\partial \zeta}{\partial x} = \rho_F D_F \frac{\partial^2 \zeta}{\partial x^2}.$$

Note that ζ is defined as

$$\zeta = -2\left(\frac{\Phi Y_F - Y_O}{\Phi + 1}\right) + \frac{\Phi - 1}{\Phi + 1}, \tag{57}$$

where Φ is the equivalence ratio. A similarity solution is obtained:

$$\zeta(x, y) = \frac{1}{2\sqrt{\pi \alpha x}} \exp\left(-\frac{y^2}{4\alpha x}\right), \tag{58}$$

where $\alpha = \frac{D_F}{u_F}$. This solution assumes infinitely fast chemistry. Since the Damkohler number in the computed solution is high (fast chemistry), the simulation results should show reasonable agreement with the similarity solution.

The initial conditions for temperature, mass fuel fraction and mass oxidizer fraction are the similarity solution. The non-dimensional pressure is set to zero and from the equation of state yields the density profile. The inlet boundary condition for temperature, density, species and velocity are set to the similarity solution. Zero derivative boundary conditions are specified at the outflow. In the y-direction, the boundary conditions are set to a constant. Since the mass flow rate is constant, this yields the u velocity profile. Again, sponge boundary condition are used and a steady state solution is obtained after the initial transient.

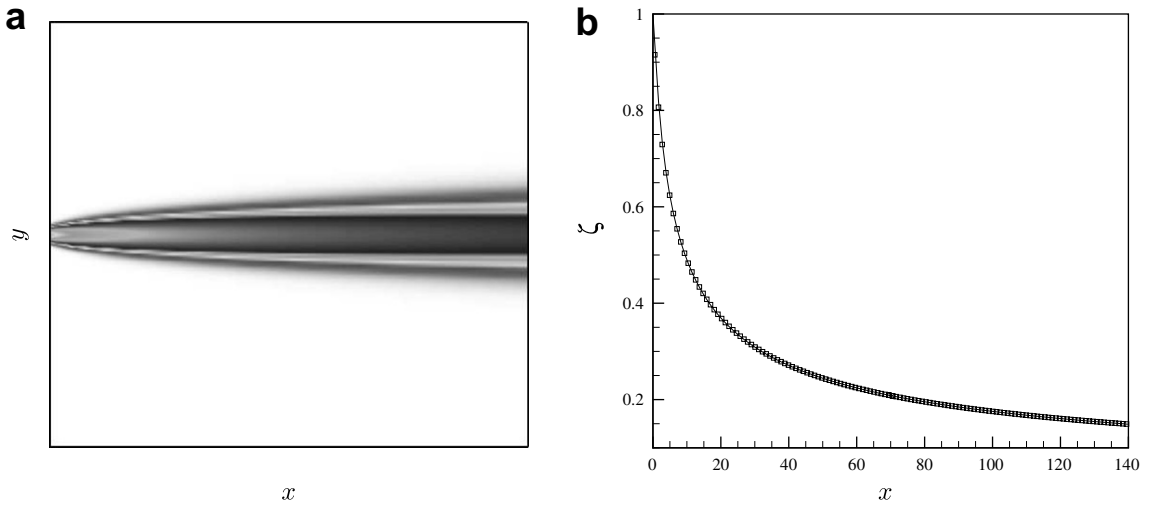

Fig. 5. (a) Contour plot of temperature for a jet flame. (b) Center line profile of the mixture fraction ζ. □ asymptotic solution from Poinsot and Veynante [5], —— numerical solution. $M_r = 0.01$, $Re = 500$, $Sc_k = Pr = 1$.

Fig. 5a shows the temperature contours of the simulation. Fig. 5b compares the similarity solution to the simulation results where the Mach number is 0.01 and the grid is 128 by 128. Note that reasonable agreement is obtained.

4.4. Turbulent non-premixed flame with one-step chemistry

A one-step diffusion flame interacting with isotropic turbulence is considered. The purpose of this calculation is to evaluate turbulence interacting with a diffusion flame at finite Mach number. The simulations are compared to Mahalingam et al. [18] and Chen et al. [19]. The simulation uses a cubic domain with inflow and outflow boundary condition in the x-direction (same as Section 4.2) and periodic boundary condition in the y and z direction. The grid uses 64 by 64 by 64 points and the Mach number is 0.1. The initial condition and parameters for the simulation are given in Table 2. From Table 2, l_t is the turbulent integral length scale and L is the length of the computational domain. δ_{fl} is the laminar flame thickness and Re_λ is the initial Taylor Reynolds number. η is the Kolmogorov scale and Da is the initial global Damkohler number defined as:

$$Da = \frac{l_t}{u_0}\left[\frac{1}{\delta_{fl}}\int_{\delta_{fl}} \dot{\omega}_T \, dx\right]. \tag{59}$$

The initial turbulence field is a three-dimensional turbulent flow where the kinetic energy spectrum is defined as

$$E(k) = C_0 \frac{u_0^2}{k_0}\left(\frac{k}{k_0}\right)^4 \exp\left[-2\left(\frac{k}{k_0}\right)^2\right], \tag{60}$$

where k is the wave number, k_0 is the wavenumber at which $E(k)$ is maximum, and u_0 is the rms velocity.

Table 2
Parameters for turbulence

Re_λ	$\frac{L}{l_t}$	$\frac{l_t}{\delta_{fl}}$	$\frac{\eta}{\delta_{fl}}$	Da
50	6	2	0.2	1

The initial diffusion flame is obtained by asymptotic solution (Cuenot and Poinsot [5]); Table 3 shows the relevant parameters. From Table 3, z_{st} is defined as $z_{st} = \frac{1}{1+\Phi}$ where Φ is the equivalance ratio. v_A and v_B are the stoichiometric coefficients. A is the pre-exponential factor. The diffusion flame is advanced in time to remove any acoustic transients. After the initial transients are removed, the initial turbulent velocity field is superimposed on the diffusion flame. The solution is advanced from 0 to 2.0 eddy turnover times and analyzed at each 0.1 eddy turnover time. Local extinction is observed to occur in the reaction rate. Holes occur in the reaction zones where pure mixing exists and the hole location corresponds to a high rate of scalar dissipation rate as predicted by laminar flamelet theory. This is shown in Figs. 6 and 7a. Fig. 7b is a contour plot of temperature showing the entire computational domain. Fig. 8 shows two-dimensional mass concentration distribution of fuel mass fraction and oxidizer mass fraction where good agreement is obtained with Chen et al. [19] (Fig. 2a in their paper). The lower bound on the species is the location of the flame and the upper bound is influenced by extinction. The distribution between the lower and upper bounds is the turbulence-induced mixing (Mahalingam et al. [18] and Chen et al. [19]).

Table 3
Parameters for diffusion flame

z_{st}	β	α	v_A	v_B	A ($m^3\ mol^{-1}\ s^{-1}$)
0.5	8	0.8	1	1	10^{12}

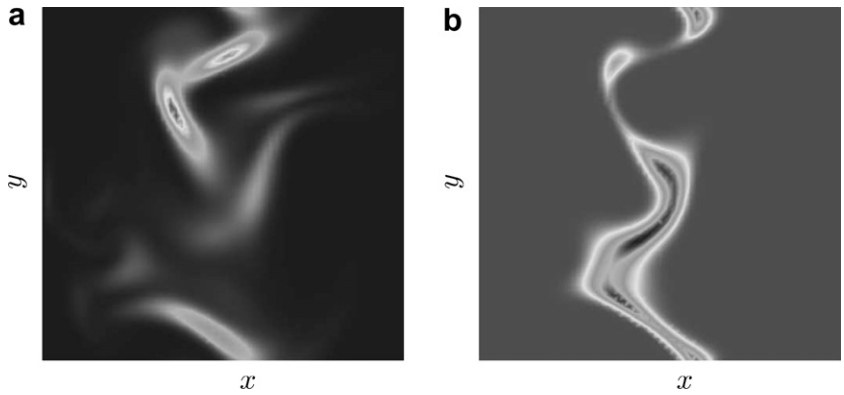

Fig. 6. (a) Scalar dissipation rate χ and (b) reaction rate $\dot{\omega}$. at $z = 4$ for turbulent diffusion flame. Notice that scalar dissipation is high where the reaction rate is low. $M_r = 0.1$, $Re = 935$, $Sc_k = Pr = 1$.

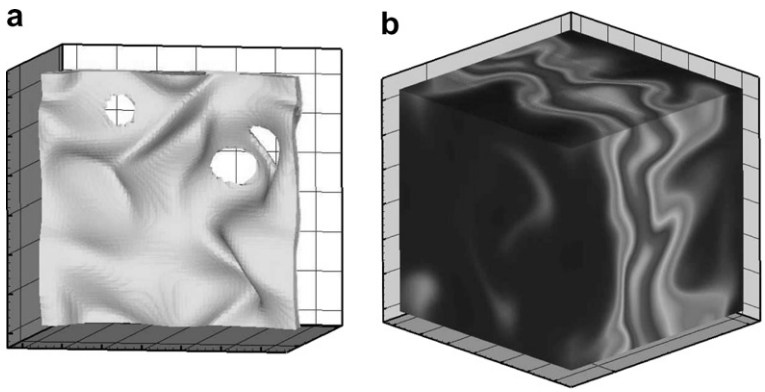

Fig. 7. (a) Iso-surface plot of the reaction rate for turbulent diffusion flame. (b) Contour plot of temperature showing entire computational domain. $M_r = 0.1$, $Re = 935$, $Sc_k = Pr = 1$.

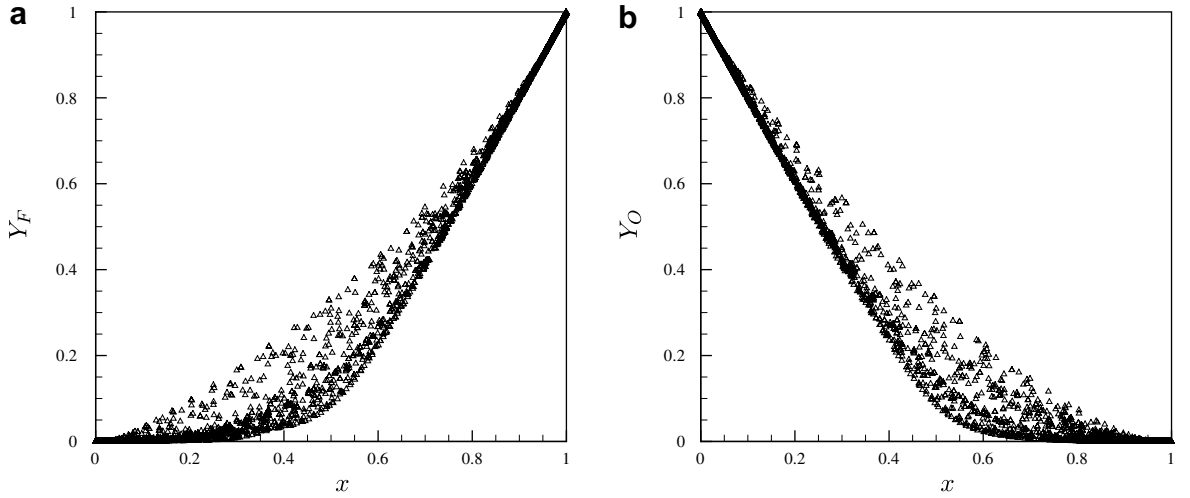

Fig. 8. Scatter plot of (a) fuel mass fraction and (b) oxidizer mass fraction from DNS of one-step, turbulent diffusion flame. $M_r = 0.1$, $Re = 935$, $Sc_k = Pr = 1$.

4.5. Modeling complex chemistry

This section illustrates application of the algorithm to complex chemistry. Combustion of H_2 and O_2 is considered, using a 9 species and 19 reaction mechanism [21]. Fig. 9 illustrates the ability of the implicit procedure described in Section 3 to handle chemical stiffness. A perfectly-stirred reactor problem is considered, the time-step is varied, and the results are compared to Chemkin [22] for accuracy. The implicit treatment of the chemical source terms allows the time-step to be five orders of magnitude higher (1.0e−3) than that possible using explicit Euler time-advancement (1.0e−8). The maximum error of the implicit solution (computed using Y_{HO_2}) compared to the explicit solution was around 5%, for $dt = 1.0e{-}3$. For $dt = 0.0001$, the percent error was around 0.01%. The ability to simulate turbulent flames involving complex chemistry is shown in Fig. 10, which shows an instantaneous realization of major and minor species from a simulation of a turbulent diffusion flame using the Mueller et al. mechanism.

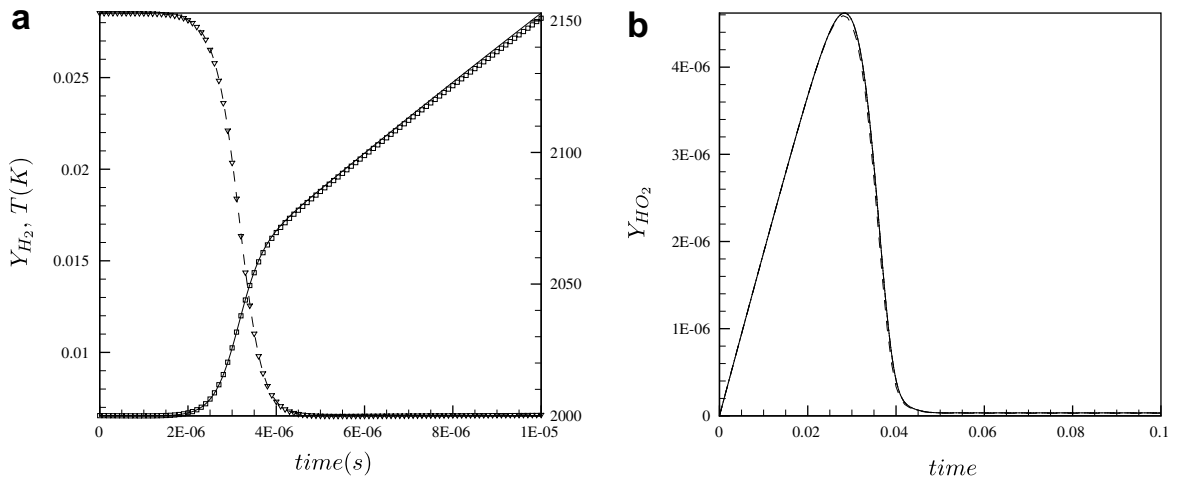

Fig. 9. (a) Comparison of a major species and temperature between Chemkin and present algorithm for a well-stirred reactor. ([T] —— Algorithm, □ Chemkin and [Y_{H_2}] in kelvin – – – Algorithm, ∇ Chemkin) (b) Illustration of the effect of time-step by comparing the explicit Euler ($dt = 1.0e{-}8$) to present implicit source term ($dt = 0.001$ and $dt = 0.0001$). – – – implicit $dt = 1.0e{-}3$, —·— implicit $dt = 1.0d-4$ ·····explicit $dt = 1.0d-8$.

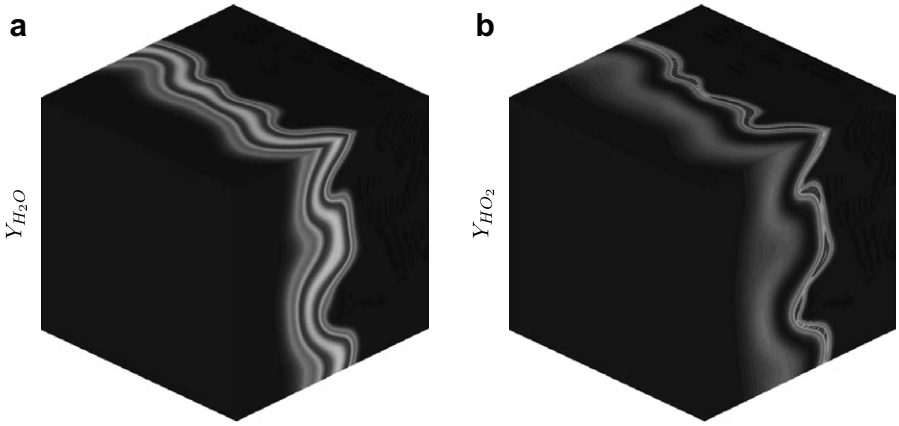

Fig. 10. Contour plots of (a) H_2O and (b) HO_2 from simulations of a turbulent diffusion flame using the Mueller et al. mechanism.

5. Summary

This paper presents a non-dissipative, implicit, robust algorithm for direct numerical and large-eddy simulation of compressible reacting flows. The method co-locates variables in space and time to allow easy extension to unstructured grids. The Navier–Stokes equations are non-dimensionalized using an incompressible scaling for pressure. From this scaling, the incompressible equations are recovered in the limit of zero Mach number and constant density. When the density varies, the zero Mach number equations for reacting flow are obtained. The discrete governing equations are discretely energy-conserving in the incompressible constant density limit [1]. The pressure, temperature, species and density are staggered in time from the velocity. This allows the algorithm to be symmetric in time. The face-normal velocity is obtained by projecting it to satisfy the energy equation. A pressure-projection approach is used. The energy equation therefore becomes an equation for the pressure-correction. The algorithm uses central differences in time and space and is second-order accurate. The species equations are implicit, and are solved separately to allow for easy extension to complex chemistry. Results are shown for premixed, diffusion flames and turbulent non-premixed flames. The numerical examples show the ability to handle chemical reaction in the limit of zero Mach number reacting flows and finite Mach number flows. The proposed method has attractive features for direct numerical and large-eddy simulation of compressible reacting flows.

Acknowledgments

This work was supported by the Air Force Office of Scientific Research under Grant FA9550-04-1-0341 and the Department of Energy under the Stanford ASC alliance. Computing resources were provided by the Minnesota Supercomputing Institute, the San Diego Supercomputing Center and the National Center for Supercomputing Applications.

References

[1] Y. Hou, K. Mahesh, A robust, colocated, implicit algorithm for direct numerical simulation of compressible, turbulent flows, J. Comput. Phys. 205 (2005) 205–221.
[2] P.A. Thompson, Compressible-fluid dynamics, McGraw-Hill, New York, 1972.
[3] H. Bijl, P. Wesseling, A unified method for computing incompressible and compressible flows in boundary-fitted coordinates, J. Comput. Phys. 141 (1998) 153–173.
[4] D.R. Van der Heul, C. Vuik, P. Wesseling, A conservative pressure-correction method for the Euler and ideal MHD equations at all speed, Intnl. J. Numer. Methods Fluids 40 (2002) 521–529.
[5] B. Cuenot, T. Poinsot, Asymptotic and numerical study of diffusion flames with variable Lewis number and finite rate chemistry, Combust. Flame 104 (1996) 111–137.
[6] T. Poinsot, D. Veynante, Theoretical and Numerical Combustion, Edwards, 2005.

[7] A. Trouve, T. Poinsot, The evolution equation for the flame surface density in turbulent premixed combustion, J. Fluid Mech. 278 (1994) 1–31.
[8] S.K. Lele, Compact finite difference schemes with spectral like resolution, J. Comput. Phys. 103 (1992) 16–42.
[9] C. Pantano, Direct simulation of non-premixed flame extinction in a methane-air jet with reduced chemistry, J. Fluid Mech. 514 (2004) 231–270.
[10] A. Majda, J.A. Sethian, The derivation and numerical solution of the equations for zero Mach number combustion, Combust. Sci. Technol. 42 (1985) 185–205.
[11] C.J. Montgomery, J.J. Riley, G. Kosaly, Direct numerical simulation of turbulent non-premixed combustion with multi-step hydrogen–oxygen kinetics, Combust. Flame 109 (1997) 113–144.
[12] C.J. Rutland, J.H. Ferziger, Unsteady strained premixed laminar flames, Combust. Sci. Tech. 73 (1990) 305.
[13] C.J. Rutland, J.H. Ferziger, Simulations of flame–vortex interactions, Combust. Flame 84 (1991) 343.
[14] C. Wall, C.D. Pierce, P. Moin, A semi-implicit method for resolution of acoustic waves in low Mach number flows, J. Comput. Phys. 181 (2002) 545–563.
[15] R.B. Pember, L.H. Howell, J.B. Bell, P. Colella, W.Y. Crutchfield, W.A. Fiveland, J.P. Jesse, An adaptive projection method for the modeling of unsteady, low-Mach number combustion, Western States Section of the Combustion Institute, 1997 Fall meeting, 1997.
[16] K. Mahesh, G. Constantinescu, P. Moin, A numerical method for large-eddy simulation in complex geometries, J. Comput. Phys. 197 (2004) 215–240.
[17] T. Echekki, J. Ferziger, A simplified reaction rate model and its application to the analysis of premixed flames, Combust. Sci. Tech. 89 (1993) 293–351.
[18] S. Mahalingam, J. Chen, L. Vervisch, Finite-rate chemistry and transient effects in direct numerical simulations of turbulent non-premixed flames, Combust. Flame 102 (1995) 285–297.
[19] J. Chen, S. Mahalingam, I.K. Puri, L. Vervisch, Effect of finite-rate chemistry and unequal Schmidt number on turbulent non-premixed flames modeled with single-step chemistry, in: CTR: Proceedings of the Summer Program, 1992, pp. 367–387.
[20] J. Chen, S. Mahalingam, I.K. Puri, L. Vervisch, Structure of turbulent non-premixed flames modeled with two-step chemistry, in: CTR: Proceedings of the Summer Program, 1992, pp. 389–402.
[21] M.A. Mueller, T.J. Kim, R.A. Yetter, F.L. Dryer, Flow reactor studies and kinetic modeling of the H_2/O_2 reaction, Int. J. Chem. Kinet. 31 (1999) 113–125.
[22] R.J. Kee, F.M. Rupley, J.A. Miller, M.E. Coltrin, J.F. Grcar, E. Meeks, H.K. Moffat, A.E. Lutz, G. Dixon-Lewis, M.D. Smooke, J. Warnatz, G.H. Evans, R.S. Larson, R.E. Mitchell, L.R. Petzold, W.C. Reynolds, M. Caracotsios, W.E. Stewart, P. Glarborg, C. Wang, C.L. McLellan, O. Adigun, W.G. Houf, C.P. Chou, S.F. Miller, P. Ho, P.D. Young, D.J. Young, D.W. Hodgson, M.V. Petrova, K.V. Puduppakkam, CHEMKIN Release 4.1, Reaction Design, San Diego, CA, 2006.